NANO LETTERS

Letter

pubs.acs.org/NanoLett

# Optomechanical Enhancement of Doubly Resonant 2D Optical Nonlinearity

Fei Yi,[§] Mingliang Ren,[§] Jason C. Reed,[§] Hai Zhu,[§] Jiechang Hou,[§] Carl H. Naylor,[∥] A. T. Charlie Johnson,[§,∥] Ritesh Agarwal,[§] and Ertugrul Cubukcu*[,†,‡,§]

[†]Department of Nanoengineering and [‡]Department of Electrical and Computer Engineering, University of California, San Diego, La Jolla, California 92093, United States

[§]Department of Materials Science and Engineering, [∥]Department of Physics and Astronomy, University of Pennsylvania, Philadelphia, Pennsylvania 19104, United States

Supporting Information

**ABSTRACT:** Emerging two-dimensional semiconductor materials possess a giant second order nonlinear response due to excitonic effects while the monolayer thickness of such active materials limits their use in practical nonlinear devices. Here, we report 3300 times optomechanical enhancement of second harmonic generation from a $MoS_2$ monolayer in a doubly resonant on-chip optical cavity. We achieve this by engineering the nonlinear light-matter interaction in a microelectromechanical system enabled optical frequency doubling device based on an electrostatically tunable Fabry−Perot microresonator. Our versatile optomechanical approach will pave the way for next generation efficient on-chip tunable light sources, sensors, and systems based on molecularly thin materials.

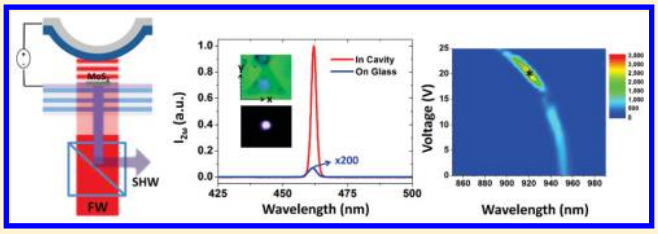


**KEYWORDS:** *Molybdenum disulfide, 2D materials, nonlinear optics, second harmonic generation, optomechanics*

Nonlinear optical materials have made possible a plethora of wavelength tunable coherent light sources crucial in many applications extending from bioimaging to laser machining. Recent studies on monolayer crystals of molybdenum disulfide ($MoS_2$) that lack inversion symmetry have confirmed that they possess a giant second order nonlinear optical response.[1−7] However, the subnanometer interaction length available for light-matter coupling in two-dimensional $MoS_2$ crystals limits their overall nonlinear conversion efficiency and prevents them from being considered in practical applications.[7]

Using photonic structures to resonantly control and enhance interaction of light with $MoS_2$ monolayers appears to be a logical step for their use in optoelectronics applications.[8−10] Optical resonators have been implemented for enhancing linear processes such as the photoluminescence from $MoS_2$.[11−15] However, to maximize the enhancement of second harmonic generation (SHG) the nonlinear nature of the light matter interaction necessitates a doubly resonant optical cavity scheme, where both the fundamental wave (FW) and the second-harmonic wave (SHW) are simultaneously resonant.[16−20] This double resonance scheme requires delicate on-chip reconfiguration of the cavity modes reminiscent of phase matching in bulk crystals. With this in mind, we have devised an integrated optomechanical frequency doubling device with a chemical vapor deposition (CVD) grown monolayer $MoS_2$ as the active nonlinear material. This microelectro-mechanical system (MEMS) enabled optical device can be electrostatically reconfigured to enhance nonlinear light generation by more than 3 orders of magnitude. The device is based on a voltage controlled widely tunable micro-Fabry−Perot (FP) cavity that consists of a spectrally selective dielectric distributed Bragg reflector (DBR) mirror and a voltage deformable silver mirror fabricated on a silicon nitride membrane as shown in Figure 1a. Figure 1b shows the multilayer stack arrangement used in our calculations for the field enhancement by the cavity and the DBR mirror consists of alternating layers of silicon nitride and oxide (see Figure S1a).

The nonlinear light-matter interaction is engineered by optomechanical tuning of the FP cavity length. This in turn controls the intracavity optical field strengths on the $MoS_2$ monolayer integrated directly on the DBR mirror designed to be highly reflective in the fundamental and second harmonic wave regions (see Figure S1b). The transparency window between these two regions allows us to clearly identify the triangular $MoS_2$ monolayer crystals from the backside of the glass substrate under the optical microscope (inset in Figure 1c). The length of integrated FP cavity can be reconfigured by applying a voltage between the metal-coated free-standing top mirror and the indium tin oxide (ITO) layer embedded in the DBR mirror as a transparent electrode (Figure 1a). The red solid line in Figure 1c shows the measured SH output intensity generated by the $MoS_2$ monolayer inside the doubly resonant

**Received:** November 1, 2015
**Revised:** February 4, 2016
**Published:** February 8, 2016





DOI: 10.1021/acs.nanolett.5b04448
*Nano Lett.* 2016, 16, 1631−1636

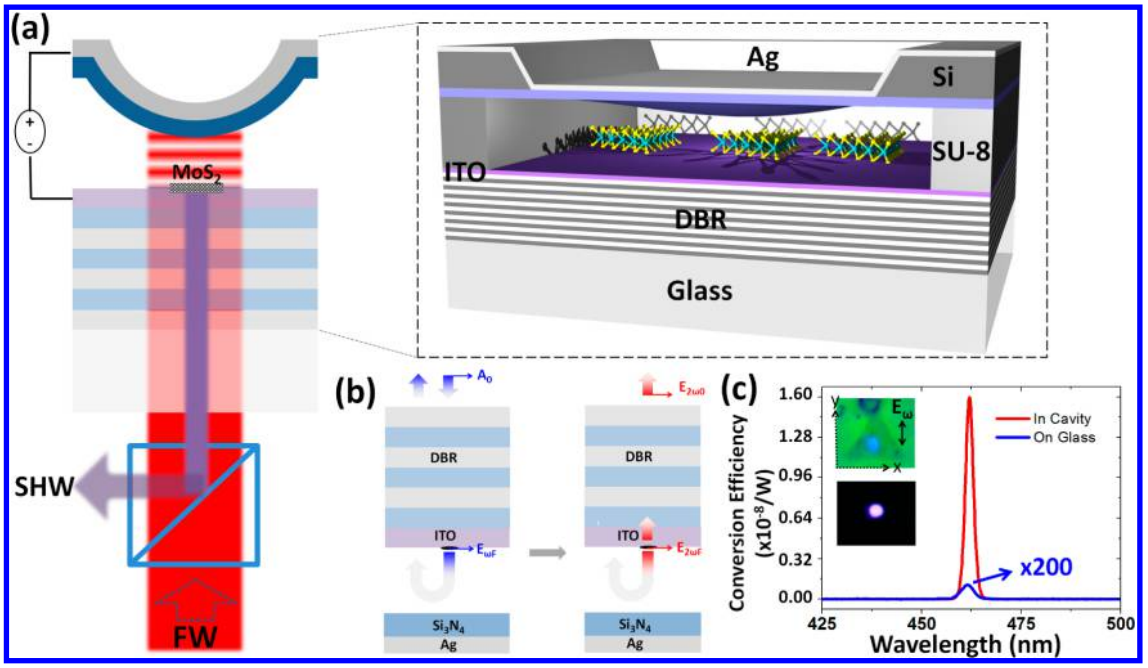


**Figure 1.** Optomechanically reconfigurable frequency doubling device. (a) Schematic of the device structure formed by the dielectric mirror on a glass substrate and a silver mirror on a suspended membrane. The silver mirror on suspended nitride membrane can be deformed by electrostatic force across the silver layer and the ITO layer, enabling the reconfiguration of the cavity. FW, fundamental wave; SHW, second harmonic wave. (b) The multilayer stack models used to calculate the cavity enhancement of the fundamental wave excitation (left) and the second harmonic wave output (right), respectively. (c) The second harmonic wave signal generated from the $MoS_2$ flake inside the cavity (red solid line) and the $MoS_2$ flake on a glass substrate (blue solid line) flake. Here the pump wavelength is 925 nm and the tuning voltage is 20 V. The insets show the spot of the second harmonic wave generated from the $MoS_2$ flakes in the cavity under bright (top) and dark (bottom) fields. The *x*-axis is defined along one of triangle sides of a CVD grown $MoS_2$, which is the zigzag direction. Therefore, the nonzero nonlinear coefficients are $\chi^{(2)} = \chi^{(2)}_{yyy} = -\chi^{(2)}_{yxx} = -\chi^{(2)}_{xxy} = -\chi^{(2)}_{xyx}$. In this work, we only focus on $\chi^{(2)}_{yyy}$.

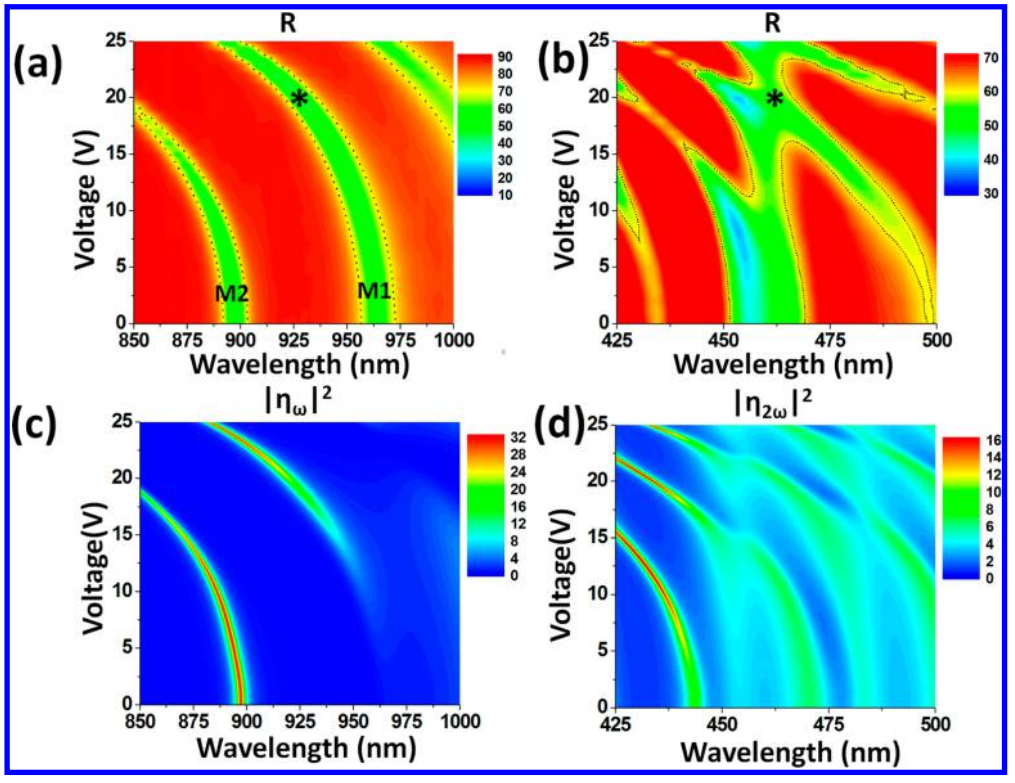


**Figure 2.** Voltage tuning of the cavity resonances. Voltage dependence of the spectral reflectance near the input fundamental (a) and output second harmonic frequencies (b), measured at the center of the device. The two FP cavity modes near the fundamental pump frequency region are labeled as $M_1$ and $M_2$. * indicates a region where a double resonance is expected. (c,d) The simulated voltage dependence of the power enhancement factors for the fundamental and the second harmonic waves, respectively.



DOI: 10.1021/acs.nanolett.5b04448
*Nano Lett.* 2016, 16, 1631−1636

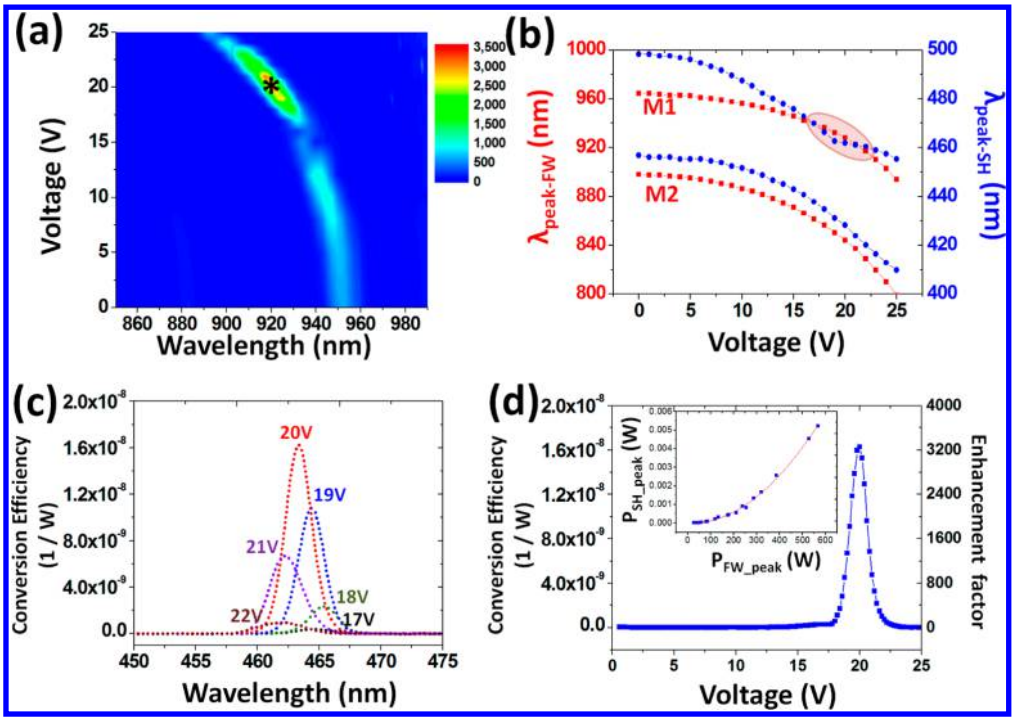


**Figure 3.** Doubly resonant second harmonic generation measurements. (a) The measured voltage dependence of the total output SHG power enhancement factor normalized to a monolayer on glass substrate. (b) The voltage dependence of the peak FP resonance wavelengths (traces from Figure 2a,b) in the fundamental (red lines) and the corresponding second harmonic (blue lines) wave regions. The crossing points in the oval between the blue and red curves indicate a double resonance region. (c) The evolution of the optical spectrum of the second harmonic wave as a function of the tuning voltage. The output peak wavelength is tunable due to the resonances narrower than the spectral pulse width of the fundamental wave fixed at 930 nm. (d) The measured voltage dependence of the total power enhancement factor and the power conversion efficiency for a pump wavelength of 930 nm. The inset shows the measured output SHG signal that is quadratically proportional to the input power.

cavity. The blue solid line shows the reference SH signal generated from a monolayer $MoS_2$ flake on a glass substrate. On the basis of this configuration, we have observed a very bright spot of SHW (~462 nm) from an individual $MoS_2$ monolayer that stood inside the cavity and was excited by FW at 925 nm (inset of Figure 1c). The normalized conversion efficiency is measured to be $1.62 \times 10^{-8}$/W (red line of Figure 1c), which is >5000 times larger than the previous literature[5] and ~3300 times stronger than that from a typical $MoS_2$ monolayer on glass (blue line of Figure 1c). Moreover, we observed that the SHG signal from $MoS_2$ in the doubly resonant cavity has a narrower linewidth compared to SHG signal from $MoS_2$ on the glass substrate (see Figure S5) and this is ascribed to the cavity enhancement. In order to gain insights on this significant phenomenon, we characterized the optomechanical tuning properties of the fabricated device. We measured the linear optical response of FP cavity under different tuning voltages to determine spectral position of the resonance modes. Figure 2a,b shows plots of the voltage dependence of spectral reflectance at the center of the device near fundamental wave and SH wave regions, respectively. It can be seen that the resonant wavelengths of the two optical modes in the fundamental wave region (marked as M1 and M2 in Figure 2a) are blue-shifted due to the decreasing cavity length by electrostatic deflection of the deformable membrane mirror. With a tuning voltage of 25 V corresponding to a 535 nm change in cavity length, M1 resonance wavelength blueshifts by 70 nm. From this blueshift, we determined the corresponding cavity length reduction, that is, mechanical deflection of the membrane, by matching the measured data with the optical transfer matrix method (TMM) calculations[21,22] (see Figure S2).

Having characterized the far-field linear response of the doubly resonant FP cavity, we need to estimate the near-field strength in the cavity to determine the nonlinear response. For this purpose, we theoretically investigate the enhancement of the second harmonic generation in the monolayer $MoS_2$ inside the FP cavity. We assume that the complex amplitude of the radiated second harmonic wave from a nonlinear monolayer flake $S_F(2\omega)$ in response to a harmonic electric field of angular frequency $\omega$ and complex amplitude $E_F(\omega)$ is given by[23] $S_F(2\omega) = \eta_F \times E_F(\omega) \times E_F(\omega)$, where $\eta_F = 4\,\mu_0\omega^2\chi^{(2)}$ is the nonlinear constant of the monolayer and $\chi^{(2)}$ is the second order nonlinear susceptibility in the plane of the material. To account for the resonant enhancement effect in the FP cavity for the fundamental wave, we define the field enhancement factor for the fundamental wave as the ratio of the fundamental electric field $E_F(\omega)$ built up at the $MoS_2$ monolayer to the incident field $A_0(\omega)$ from outside the cavity, $\eta_\omega = E_F(\omega)/A_0(\omega)$. Figure 2c shows the calculated intensity enhancement factor of the fundamental wave (defined as $|\eta_\omega|^2$) as a function of wavelength and voltage (see Supporting Information for the details of calculation). It can be seen that the resonant wavelengths of the cavity modes can be blue-shifted through voltage tuning while the enhancement factor $|\eta_\omega|^2$ can be tuned up to 30 times. Similar to the fundamental wave, the radiated second harmonic wave also builds up in the resonant cavity. We define the field enhancement factor $\eta_{2\omega}$ for the second harmonic wave as the ratio of the output electric field $S_0(2\omega)$ at the second harmonic frequency to the radiated second


DOI: 10.1021/acs.nanolett.5b04448
Nano Lett. 2016, 16, 1631−1636

harmonic electric field from the $MoS_2$ flake $S_F(2\omega)$: $\eta_\omega = S_0(\omega)/S_F(\omega)$.

Figure 2d shows that the intensity enhancement factor for the second harmonic wave $|\eta_{2\omega}|^2$ can also be tuned by changing the cavity length. The total power enhancement factor by the cavity is then characterized by $|\eta_{2\omega}|^2 \times |\eta_\omega|^4$. Because the intracavity power is proportional to the quality factor, this result is consistent with calculations from coupled mode theory for doubly resonant cavities under critical coupling conditions.[23,24] In this case, the nonlinear output power qualitatively scales with $(Q_\omega)^2 \times (Q_{2\omega})$, where $Q_\omega$ and $Q_{2\omega}$ are the quality factors for the fundamental and second harmonic waves, respectively.[23,24] Our TMM calculation predicts that the total second harmonic output power can be enhanced above 3500 times through voltage tuning the cavity to attain double resonance (see Figure S6 for details). This maximum enhancement corresponds to the case where both the fundamental and second harmonic waves are spectrally tuned with two cavity modes, that is, double resonance condition.

To test our theoretical predictions, we experimentally characterized the nonlinear conversion efficiency of the fabricated device. For excitation, we use transform limited pulses with a duration of 140 fs. For different tuning voltages, we scan the pulse center wavelength in the 850−1000 nm window corresponding to the region where the micro-FP cavity supports fundamental wave resonances. This allows us to map the overall optomechanical power enhancement factor of SHG that is the ratio between SHG signals from a $MoS_2$ monolayer in our cavity device and from a typical $MoS_2$ monolayer on a glass, as shown in Figure 3a. The measured data agree well with the theoretical results (see Figure S6). For a pump wavelength of 925 nm and a tuning voltage of 17 V, the measured maximum enhancement is 3300 times larger than the SHG from a monolayer on a glass substrate. This set of parameters corresponds to the doubly resonant cavity case as shown in Figure 3b, where the fundamental and second harmonic wavelengths overlap spectrally with two separate cavity resonances. It can be seen that the traces for cavity resonances near the fundamental and second harmonic frequencies intersect in that region when a 17 V tuning bias is applied unlike the mismatched case for 0 V. (See Figure S3 for the voltage tuning of the spectral reflectance in both the FW region and the SH region.) This is reminiscent of phase matching for copropagating beams in bulk birefringent nonlinear materials. For other combinations of tuning voltage and fundamental wavelength, the nonlinear enhancement is not significant. Singly resonant coupling is also observed when only the fundamental wavelength is resonant with M1 and the second harmonic wavelength is spectrally mismatched from a cavity mode. Similarly, when the fundamental wavelength follows M2, the enhancement is 30× weaker due to lack of a double resonance condition.

We also characterized the absolute conversion efficiency ($P_{2\omega}/P_\omega^2$, see Methods) of the second harmonic generation. Figure 3c shows the evolution of the optical spectrum of the second harmonic wave as a function of the tuning voltage. The output SHG peak wavelength can be tuned slightly by voltage because the cavity modes are spectrally narrower than the incident fundamental pulse width (Figure S5). Our unique nonlinear device configuration also allows us to dynamically control the output of this frequency doubler with voltage. Figure 3d plots the voltage dependence of the measured power conversion efficiency and enhancement factor when the fundamental wave is fixed at 930 nm.

On the contrary, the light-matter interactions in this device can be completely turned off by an applied voltage that detunes the fundamental cavity resonance from the pump. This enables the full optomechanical control of the SHG output intensity for a given input wavelength and optical power. Also, the SHG signal is switched from ON state at 20 V to completely OFF state at 22.5 V, indicating the very efficient tuning capability of our cavity (40% per volt). Because of the capacitive nature, this frequency doubler will not consume any energy for static switching operations. The inset in Figure 3d shows the SHG output power as a function of the input pump power for the double resonance condition from which we calculate the power conversion efficiency to be $1.62 \times 10^{-8}$/W, which is 5000 larger than reported value measured from $MoS_2$ flake on a $Si/SiO_2$ (280 nm) substrate.[5] The measured modulation cutoff frequency for this proof-of-concept-device was 200 Hz limited by the driving electronics (see Figure S4). These devices can be modulated resonantly at much higher frequencies if driven at one of the acoustic resonances supported by the membrane mirror.[25]

In summary, we demonstrated optomechanical enhancement of effective nonlinear optical response in monolayer $MoS_2$ crystals in a versatile nonlinear device platform based on doubly resonant optical cavities. This on-chip voltage controlled frequency doubling device can address the short nonlinear interaction lengths in emerging two-dimensional materials. We envision that our strategy of on-chip nanoscale opto-electro-mechanical integration will lead to next generation tunable nonlinear light sources and devices.

**Methods.** *Sample Preparation.* The DBR was fabricated by plasma-enhanced chemical vapor deposition (PECVD, Oxford PlasmaLab 100) on a glass slide after 10 min sonication cleaning in acetone and IPA. Layer stacking of DBR first consists of eight pairs of 130 nm SiNx/130 nm SiOx thin film deposition. Then a layer of ∼50 nm ITO was deposited on top as-fabricated DBR structure by DC magnetron sputtering (Explorer 14) under 5 mTorr at 450 W with $Ar/O_2$ ratio as 100:3.

The refractive indices of the ITO and the PECVD SiNx and SiOx thin films are characterized using Filmmetrics F40. A 1.5 $\mu$m thick SU-8 layer is then spin-coated and patterned on top of the ITO layer as the spacer. A commercially available silicon nitride window with 100 nm thick membrane bonded on top of the SU-8 spacer through commercially available adhesive (cyanoacrylate). The backside of the membrane is precoated with a 50 nm of silver layer at the backmirror through e-beam evaporation. Electrical contacts to the MEMs capacitor are through the silver layer and the ITO layer, respectively.

*$MoS_2$ Growth.* Single crystal $MoS_2$ flakes were grown directly on a 300 nm $SiO_2/Si$ substrate by chemical vapor deposition. A 1% sodium cholate solution is initially spin coated onto the $SiO_2$ substrate to help promote a growth region. A microdroplet of a saturated solution of ammonium heptamolybate (AHM) is deposited onto the corner of the substrate. The AHM will act as the molybdenum feedstock. The substrate is placed in the center of a 1 in. Lindberg blue furnace and 25 mg of solid sulfur (part number 213292, Sigma-Aldrich) is placed upstream at a distance of 18 cm from the growth substrate. Nitrogen at 700 sccm is flown through the chamber and the temperature of the furnace is ramped up to 800 C; the sulfur pellet is heated up to 150 °C. After a 30 min growth, the


DOI: 10.1021/acs.nanolett.5b04448
Nano Lett. 2016, 16, 1631−1636

furnace is then stopped and rapidly cooled to room temperature. The growth substrate is retrieved and $MoS_2$ flakes were grown across the $SiO_2$ substrate.

*Characterization of the Optomechanical Resonant Cavity.* We first measured the voltage-dependent spectral reflectance of the FP-cavity at the center of the device using Filmmetrics F40. The corresponding voltage controlled cavity length is then determined by fitting the simulated spectral reflectance (by transfer matrix method) with the measured spectral reflectance. We then simulated the voltage controlled mechanical deflection of the silver-coated silicon nitride membrane in the MEMs capacitor using the electromechanics module in COMSOL 4.4 and compared it with the voltage controlled cavity length determined by the spectral reflectance measurement to predict the pull-in voltage of the MEMs capacitor.

*Characterization of Optomechanically Enhanced 2D Nonlinearity.* A femtosecond-pulsed Ti:sapphire laser (Chameleon), tuned from 680 to 1000 nm with ∼140 fs pulse width and 80 MHz repetition rate, was focused onto individual flakes through the DBR mirror by means of a home-built microscope equipped with a 10×, 0.25 NA objective (Nikon). The average excitation power of ∼2 mW (FW) was used to excite SHG from the $MoS_2$ flakes. The SHG signals were imaged by a cooled charge-coupled device and measured by a spectrometer (Acton) with a spectral resolution of 0.1 nm. The external normalized conversion efficiency is defined as $P_{2\omega}/P_{\omega}^2$ where $P_{\omega}$ is the peak power of FW illuminated upon the DBR mirror while $P_{2\omega}$ is the peak power of generated SHW coming out from the cavity. The reported conversion efficiency (e.g., $1.68 \times 10^{-8}$/W) has considered the system collection efficiency,[26] including transmission/reflection coefficient of each optical elements. The measured power enhancement factor is defined as the SH power from the cavity normalized to the SH power from the $MoS_2$ monolayer on a glass substrate.

## ■ ASSOCIATED CONTENT

### Supporting Information

The Supporting Information is available free of charge on the ACS Publications website at DOI: 10.1021/acs.nanolett.5b04448.

Theoretical analysis of the resonant optical cavity; the structure and spectral reflectance of the distributed bragg reflector; voltage-dependent mechanical deflection of the membrane mirror; voltage-dependent spectral reflectance of the optomechanical resonant cavity; measurement of the modulation speed of the optomechanical cavity; characterization of the quality factor of resonant cavity; the optical field distribution inside the cavity at resonances; comparison of power enhancement factors of $MoS_2$ in cavity and $MoS_2$ on glass; the second harmonic wave output intensity from the cavity as a function of the nonlinear layer thickness; estimation of the theoretical quality factors of the micro-FP on double resonance. (PDF)

## ■ AUTHOR INFORMATION


### Corresponding Author

*E-mail: ecubukcu@ucsd.edu.

### Author Contributions

F.Y. and M.R. contributed equally.


### Notes

The authors declare no competing financial interest.

## ■ ACKNOWLEDGMENTS

This work was supported by NSF under the NSF 2-DARE program (EFMA-1542879), by the ECCS division (Mahmoud Fallahi) under award number ECCS-1408139, and partially by the MRSEC Program under award number DMR11-20901. R.A. was supported by the U.S. Army Research Office under Grant W911NF-11-1-0024.

## ■ REFERENCES


(1) Yin, X. B.; Ye, Z. L.; Chenet, D. A.; Ye, Y.; O'Brien, K.; Hone, J. C.; Zhang, X. *Science* **2014**, *344* (6183), 488−490.

(2) Malard, L. M.; Alencar, T. V.; Barboza, A. P. M.; Mak, K. F.; de Paula, A. M. *Phys. Rev. B: Condens. Matter Mater. Phys.* **2013**, *87* (20), 201401.

(3) Mai, C.; Semenov, Y. G.; Barrette, A.; Yu, Y.; Jin, Z.; Cao, L.; Kim, K. W.; Gundogdu, K. *Phys. Rev. B: Condens. Matter Mater. Phys.* **2014**, *90* (4), 041414.

(4) Seyler, K. L.; Schaibley, J. R.; Gong, P.; Rivera, P.; Jones, A. M.; Wu, S.; Yan, J.; Mandrus, D. G.; Yao, W.; Xu, X. *Nat. Nanotechnol.* **2015**, *10* (5), 407−411.

(5) Kumar, N.; Najmaei, S.; Cui, Q.; Ceballos, F.; Ajayan, P. M.; Lou, J.; Zhao, H. *Phys. Rev. B: Condens. Matter Mater. Phys.* **2013**, *87* (16), 161403.

(6) Li, Y.; Rao, Y.; Mak, K. F.; You, Y.; Wang, S.; Dean, C. R.; Heinz, T. F. *Nano Lett.* **2013**, *13* (7), 3329−3333.

(7) Hsu, W.-T.; Zhao, Z.-A.; Li, L.-J.; Chen, C.-H.; Chiu, M.-H.; Chang, P.-S.; Chou, Y.-C.; Chang, W.-H. *ACS Nano* **2014**, *8* (3), 2951−2958.

(8) Furchi, M.; Urich, A.; Pospischil, A.; Lilley, G.; Unterrainer, K.; Detz, H.; Klang, P.; Andrews, A. M.; Schrenk, W.; Strasser, G.; Mueller, T. *Nano Lett.* **2012**, *12* (6), 2773−2777.

(9) Engel, M.; Steiner, M.; Lombardo, A.; Ferrari, A.; Loehneysen, H.; Avouris, P.; Krupke, R. *Nat. Commun.* **2012**, *3*, 906−906.

(10) Liu, X.; Galfsky, T.; Sun, Z.; Xia, F.; Lin, E.-c.; Lee, Y.-H.; Kéna-Cohen, S.; Menon, V. M. *Nat. Photonics* **2014**, *9* (1), 30−34.

(11) Butun, S.; Tongay, S.; Aydin, K. *Nano Lett.* **2015**, *15* (4), 2700−2704.

(12) Gan, X.; Gao, Y.; Fai Mak, K.; Yao, X.; Shiue, R.-J.; van der Zande, A.; Trusheim, M. E.; Hatami, F.; Heinz, T. F.; Hone, J.; Englund, D. *Appl. Phys. Lett.* **2013**, *103* (18), 181119.

(13) Schwarz, S.; Dufferwiel, S.; Walker, P. M.; Withers, F.; Trichet, A. A. P.; Sich, M.; Li, F.; Chekhovich, E. A.; Borisenko, D. N.; Kolesnikov, N. N.; Novoselov, K. S.; Skolnick, M. S.; Smith, J. M.; Krizhanovskii, D. N.; Tartakovskii, A. I. *Nano Lett.* **2014**, *14* (12), 7003−7008.

(14) Sobhani, A.; Lauchner, A.; Najmaei, S.; Ayala-Orozco, C.; Wen, F.; Lou, J.; Halas, N. J. *Appl. Phys. Lett.* **2014**, *104* (3), 031112.

(15) Lee, J.; Tymchenko, M.; Argyropoulos, C.; Chen, P.-Y.; Lu, F.; Demmerle, F.; Boehm, G.; Amann, M.-C.; Alu, A.; Belkin, M. A. *Nature* **2014**, *511* (7507), 65−69.

(16) Ashkin, A.; Boyd, G. D.; Dziedzic, J. *IEEE J. Quantum Electron.* **1966**, *2* (6), 109−124.

(17) Simonneau, C.; Debray, J. P.; Harmand, J. C.; Vidakovi, P.; Lovering, D. J.; Levenson, J. A. *Opt. Lett.* **1997**, *22* (23), 1775−1777.

(18) Ou, Z. Y.; Kimble, H. J. *Opt. Lett.* **1993**, *18* (13), 1053−1055.

(19) Bi, Z.-F.; Rodriguez, A. W.; Hashemi, H.; Duchesne, D.; Loncar, M.; Wang, K.-M.; Johnson, S. G. *Opt. Express* **2012**, *20* (7), 7526−7543.

(20) Rodriguez, A.; Soljacic, M.; Joannopoulos, J. D.; Johnson, S. G. *Opt. Express* **2007**, *15* (12), 7303−7318.

(21) Yeh, P. *Optical Waves in Layered Media*; Wiley: New York, 1988; Vol. *95*.

(22) Ren, M.-L.; Li, Z.-Y. *J. Opt. Soc. Am. B* **2010**, *27* (8), 1551−1560.

(23) Berger, V. *J. Opt. Soc. Am. B* **1997**, *14* (6), 1351−1360.




DOI: 10.1021/acs.nanolett.5b04448
*Nano Lett.* 2016, 16, 1631−1636

(24) Liscidini, M.; Claudio Andreani, L. *Phys. Rev. E* **2006**, *73* (1), 016613.
(25) Yi, F.; Zhu, H.; Reed, J. C.; Cubukcu, E. *Nano Lett.* **2013**, *13* (4), 1638−1643.
(26) Ren, M. L.; Liu, W. J.; Aspetti, C. O.; Sun, L. X.; Agarwal, R. *Nat. Commun.* **2014**, *5*, 5432.



DOI: 10.1021/acs.nanolett.5b04448
*Nano Lett.* 2016, 16, 1631−1636